Bioactive Constituents, Metabolites, and Functions

Novel Flaxseed Gum Nanocomposites are Slow Release Iron Supplements

Shan Liang, Yu Huang, Youn Young Shim, Xiang Ma, Martin John Tarsisius Reaney, and Yong Wang

J. Agric. Food Chem., **Just Accepted Manuscript** • DOI: 10.1021/acs.jafc.8b01347 • Publication Date (Web): 08 May 2018

Novel Flaxseed Gum Nanocomposites are Slow Release Iron Supplements

Shan Liang,[†,‡] Yu Huang,[†,‡] Youn Young Shim,[†,§] Xiang Ma,[‖] Martin J. T. Reaney,[†,§] Yong Wang[*,†,‡]

[†] Guangdong Saskatchewan Oilseed Joint Laboratory, Department of Food Science and Engineering, Jinan University, Guangzhou, Guangdong 510632, China

[‡] Guangdong Engineering Technology Research Center for Oils and Fats Biorefinery, Guangzhou, Guangdong 510632, China

[§] Department of Plant Sciences, University of Saskatchewan, 51 Campus Drive, Saskatoon, Saskatchewan S7N 5A8, Canada

[‖] Division of Chemistry & Chemical Engineering, California Institute of Technology, 1200E California Blvd., Pasadena, CA 91125, USA

ABSTRACT: Nanocomposites, based on iron salts and soluble flaxseed gum (FG), were prepared as potential treatments of iron deficiency anemia (IDA). FG was extracted, characterized, and formulated into iron-loading nanocomposites *via* ion-exchange against $FeCl_3$, $Fe_2(SO_4)_3$, $FeCl_2$ and $FeSO_4 \cdot 7H_2O$. FG-iron nanocomposites preparation condition was optimized, and physicochemical properties of the nanocomposites were investigated. *In vitro* release kinetics of iron in simulated gastric fluid (SGF) were also evaluated. FG heteropolysaccharide consisting of rhamnose (33.73%), arabinose (24.35%), xylose (14.23%), glucose (4.54%), and galactose (23.15%) monosaccharides, linked together *via* varieties of glycosidic bonds, was a good recipient for both ferric and ferrous irons under screened conditions (i.e. 80 °C, 2 h, I:G = 1:2). Iron loaded contents in the nanocomposites prepared from FG-$FeCl_3$, FG-$Fe_2(SO_4)_3$, FG-$FeCl_2$, and FG-$FeSO_4 \cdot 7H_2O$ were 25.51%, 10.36%, 5.83%, and 22.83%, respectively. Iron in these nanocomposites was mostly in a bound state, especially in FG-$FeCl_3$, due to chelation forming bonds between iron and polysaccharide hydroxyl or carboxyl groups and formed stable polysaccharide-iron crystal network structures. Free iron ions were effectively removed by ethanol treatments. Due to chelation, the nanocomposites delayed iron release in SGF and the release kinetics were consistent with Korsmeyer-Peppas model. This indicates that such complexes might reduce side effects of free iron in human stomach. Altogether, this study indicates that these synthetic FG-iron nanocomposites might be developed as novel iron supplements for iron deficiency, in which FG-$FeCl_3$ is considered as the best option.

KEYWORDS: *flaxseed gum, nanocomposite, iron supplement, simulated digestion, release kinetics*

INTRODUCTION

Iron is an essential trace element with unique physiological and pharmacological functions in the human body. It is critical in maintaining organism homeostasis, particularly, iron is an essential cofactor involved in metabolism (e.g. oxygen transport, drug metabolism, steroid synthesis, DNA synthesis, ATP production, and electron transport) and immune function.[1–3] Iron deficiency increases the risk of iron-deficiency anemia (IDA), coronary artery disease, heart failure, pulmonary hypertension, bleeding, inflammatory disease, and Plummer-Vinson syndrome.[4,5] Recent studies suggest that iron deficiency malnutrition affects up to 2 billion people worldwide.[5] A report from the World Health Organization estimated that 46% of the world's 5- to 14-year-old children and 48% of the pregnant women are anemic, in which approximately 50% of these cases are due to iron deficiency, especially in developing countries.[6,7] IDA could arise from insufficient iron intake, poor iron bioavailability, increased iron demands, chronic blood loss, parasitic infection, or chronic inflammatory.[1,8] Oral or intravenous injection of iron supplements are the most common methods of iron administration in treating or preventing IDA in human that have long been accepted by the public.[9]

Traditionally, ferrous sulfate is the main supplement used in the treatment of iron deficient related diseases, including IDA. However, these supplements often induce undesired side effects including gastrointestinal allergic reactions and discomfort (e.g. nausea, vomiting, constipation, diarrhea and epigastric pain).[10–12] Furthermore, free Fe^{2+} can cause oxidative damage to cell membranes through the formation of free radicals.[13] Additionally, iron supplements can be toxic when the iron intake is higher than the amount required for sustainability.[14] These symptoms vary proportionally to the concentration of ionizable iron in the upper gastrointestinal tract and can be reduced by ingestion of iron with food or using a chelated form.[15] Therefore, it is necessary to develop new types of iron delivery mechanisms with reduced side effects, to replace ferrous sulfate based iron supplements.

Polysaccharide-iron complex, e.g. Niferex, *Astragalus membranaceus* polysaccharide-iron (III)

complex, inulin-iron complexes, tea polysaccharides-iron complex, and *Inonotus obliquus* polysaccharide-iron (III) complex, etc., are an excellent alternative for IDA treatment as they mitigate side effects, have high water-solubility, stability, and relative low toxicity.[16] In recent years, investigations into the potential treatment of IDA using these polysaccharide-iron complexes have become a topic of intense study.[1,14,15,17] Such complexes can maintain relatively high concentrations of iron at physiological pH in a soluble and nontoxic form, thereby acting as an effective donor of iron *in vivo*.[18] In fact, non-starch polysaccharides (e.g. some food hydrocolloids) generally have the ability to bind cations (e.g. Fe^{2+} and Fe^{3+}) *in vitro* as a consequence of their polyanionic nature.[19] Therefore, polysaccharide substances, including gum, mucilage and hydrocolloids, can be used as potential receptors for free iron to form a chelate complex.

Flaxseed gum (FG), a main component of flaxseed, is mainly comprised of a small amount of protein and massive polysaccharides that consisting of a neutral fraction (arabinoxylans) and an acidic fraction (rhamnogalacturonans).[20,21] Soluble FG occurs mainly at the outermost layer of the hull. This fibre-rich hull is able to release mucilaginous material (soluble gum) easily when soaked in water. FG can be used as an additive in food, cosmetic and pharmaceutical industries due to its excellent rheological properties including thickening, emulsification, and gelling.[22,23] However, the application of FG in the synthesis of functional nanocomposites is rarely reported. In recent years, nanocomposites of natural carbohydrate polymers (e.g. chitosan, xanthan gum, and carboxymethyl cellulose) have been a subject of comprehensive research because these compounds demonstrated exceptional biocompatibility and physiochemical properties.[24–26] Therefore, as a natural soluble plant seed mucilage comprising mainly of polysaccharide substances, FG can potentially act as an excellent resource for preparing iron-loaded nanocomposites. The application of FG as a chelating agent for the complexation of iron ions into nanocomposite structures could redefine current strategies in the treatment of iron deficiency related diseases.

In this study, we developed four novel iron-loading nanocomposites based on soluble FG through

ion-exchange against $FeCl_3$, $Fe_2(SO_4)_3$, $FeCl_2$, and $FeSO_4 \cdot 7H_2O$, followed by repeated ethanol washes to remove free iron. Nanocomposites preparation conditions were compared, and the physicochemical properties of better nanocomposites were characterized by chemical and instrumental methods. Finally, *in vitro* iron release kinetics of the nanocomposites in simulated gastric fluid (SGF) were investigated. Based on the results obtained in this study, we will develop novel iron supplements that induce minimal side effects and might be used as potential treatments of IDA.

MATERIALS AND METHODS

Materials and reagents. Flaxseed (*Linum usitatissimum* L., var. CDC Sorrel), was generously provided from Dr. Helen Booker (University of Saskatchewan) and harvested from Floral (SK, Canada) in 2015. Seeds were kept in a desiccator at room temperature (~23 °C) for subsequent studies. All chemicals and reagents used in this study were of analytical grade. Iron salts: $FeCl_3$, $Fe_2(SO_4)_3$, $FeCl_2$, $FeSO_4 \cdot 7H_2O$, potassium thiocyanate (KSCN) and 1,10-phenanthroline, were purchased from Sigma-Aldrich Canada Ltd. (Oakville, ON, Canada). Analytical monosaccharide standards, D-xylose, L-fucose, L-rhamnose, L-arabinose, D-galactose, D-glucose and D-mannose, were purchased from Sigma-Aldrich Shanghai Trading Co., Ltd. (Shanghai, China). SGF was prepared by dissolving 2.0 g NaCl, 7 mL HCl (37%) and 3.2 g pepsin (Aladdin Shanghai Biochemical Technology Co., Ltd., Shanghai, China) in 1 L deionized water, in which the pepsin was added 45 min before the simulated digestion experiment running.

FG extraction. Whole seeds were milled using a small household vegetable juicer (GSE-5050, Corrupad Korea Co., Ltd., Korea), then degreased using 95% ethanol at 60 °C, and finally separated into flaxseed hull, kernel and oil using a “wet screening method”. Briefly, the suspend mixture of degreasing system was fleetly screened by a 425 μm sieve. Flaxseed kernel formed fine particles in the decreasing system so that passed through the sieve with ethanol extract. Flaxseed hull with larger size was retained on the sieve, thereafter collected and vacuum dried. FG were extracted from the flaxseed hull using a hot water

extraction method.[27] Briefly, flaxseed hull was treated by hot water (80 °C) twice (2 h per time) under an initial material-to-liquid ratio of 1:50, followed by a subsequent treatment of material-to-liquid ratio of 1:30. This solution was then subjected to filtration and ethanol precipitation prior to being redissolved in deionized water and lyophilized at –50 °C for 24 h to prepare the FG for nanocomposites synthesis.

Structure identification of FG. *Monosaccharide composition analysis.* Monosaccharide composition analysis of FG was conducted using gas chromatography (GC) methodology after derivatization with aldononitrile acetate.[28,29] Briefly, 10 mg of FG was hydrolyzed by 4.0 M trifluoroacetic acid for 4 h at 120 °C. The hydrolysate was then subjected to derivatization of aldononitrile acetate by reacting with hydroxylamine, acetic anhydride, and pyridine hydrochloride successively. The compounds of interest were then extracted from the solution, using methylene chloride, prior to GC analyses. The derivatizations of monosaccharide standards were carried out simultaneously. DB-1701 GC capillary column (30 m × 0.25 mm, 0.25 μm, J&W Scientific, Folsom, CA, USA) was employed to analyse the monosaccharide composition according to the reported temperature gradients: column temperature was kept at 190 °C for 2 min, increased to 240 °C with a speed of 2 °C/min, and then kept at 240 °C for 2 min.[29]

Nuclear magnetic resonance (NMR) analysis. Thirty milligrams of FG was fully dissolved in 6.0 mL D_2O and 0.6 mL of the mucilage was transferred into a 5 mm i.d. NMR tube. ^{1}H- and ^{13}C-NMR spectra of FG were recorded on a 600 MHz Advance NMR spectrometer (Bruker BioSpin Corp., Billerica, MA, USA) at room temperature. The unprocessed free induction decay (fid) data were then converted into a frequency domain by Fourier transform software (TopSpin 3.2, Bruker BioSpin Corp., Billerica, MA, USA).

Synthesis of the FG-iron nanocomposites. One hundred milligrams of FG was dissolved in 15 mL deionized water overnight under continuous stirring, followed by addition of 5.0 mL of a defined concentration of iron solution (i.e. $FeCl_3$, $Fe_2(SO_4)_3$, $FeCl_2$, and $FeSO_4 \cdot 7H_2O$). Reactions were performed in a fully automatic reactor (Synthesis 1 liquid, 25 mL, Heidolph Instruments GmbH, Schwabach, Germany),

in which the reaction temperature and time were controllable and predefined, to determine the optimal screening conditions. At the end of the reaction, the FG-iron complex mixtures were precipitated, overnight with four volumes of absolute ethanol, to remove free iron and other ethanol-soluble molecules. The precipitate was separated from the ethanol solution *via* centrifugation at 3500 rpm for 5 min. To ensure the efficient removal of free iron ions in the complexes, the mixture was washed with 80% (*v*/*v*) ethanol in water (3 × 40 mL) followed by centrifugation using the above parameters. Products were then baked at 60 °C overnight and the dried product was ground in an agate mortar to get the final FG-iron nanocomposites. The best reaction conditions were screened using small-scale experiments with the main evaluation indices monitoring for iron content and product yields.

An expanded pilot study was also conducted where 2 g FG was used, and the reaction was performed in a 500 mL round bottom flask immersed in a hot water bath (DF-101S, Gongyi Yu Hua Instrument Co., Ltd., Henan, China) under previously screened reaction conditions. Subsequent sample processing was identical to the previous condition-screened experiments except the samples were dried *via* lyophilization for 24 h, rather than baked at 60 °C in an oven.

Qualitative and quantitative identification of iron. *Qualitative identification of free iron.* Colorimetric analyses using KSCN and 1,10-phenanthroline were performed for qualitative identification of Fe^{3+} and Fe^{2+}, respectively.[30,31] This methodology measured the effectiveness of free iron removal from the synthetic nanocomposites accomplished through ethanol precipitating and washing. For the qualitative identification of the final FG-iron nanocomposites, 2.0 mg product was dissolved in a solution containing 2 mL of 1.0 M HCl acid or 2 mL deionized water for 24 h, and vortexed every 6 h. Afterwards, 1.0 mL nanocomposites solutions were transferred into a 10 mL vial and diluted with 5.0 mL deionized water, prior to colorimetric analyses using KSCN and 1,10-phenanthroline.

Quantification of iron content. The quantification of total iron content was completed, with minor

modifications, as suggested by Pitarresi, et al., 2008.[15] Briefly, 2.0 mg dried FG-iron nanocomposites were dispensed into 2.0 mL of 1.0 M HCl for 24 h, and vortexed every 6 hours, in order to break the chelated complex and release the iron. Each sample (0.2 mL) was then mixed with 0.80 mL deionized water, 1.0 mL of 10% hydroxylamine hydrochloride, 1.0 mL of 0.25% (*w*/*v*) 1,10-phenanthroline and 5.0 mL sodium acetate trihydrate buffer solution (pH 4.5) and incubated for 15 mins at room temperature, prior to absorbance measurement *via* UV-vis analyses (performed at λ = 510 nm). Ferrous ammonium sulfate was used as the analytical standard and to produce the calibration curve. Free iron content was analysed similarly, except samples were dispensed in 2.0 mL deionized water and vortexed every 6 h for 24 h. Combined iron content was calculated as the difference between total iron and free iron content. Finally, for the quantification of ferrous iron content, samples were also dispensed in 2.0 mL HCl (1.0 M) for 24 h and an equal volume of deionized water was added instead of 10% hydroxylamine hydrochloride in the pretreatment system. Ferric iron content was calculated as the difference between total iron and ferrous iron content.

Product yields calculation. Product yields were calculated according to the following equation:

$$\text{Product yield (\%)} = \frac{\text{Product weight (mg)}}{\text{FG weight (mg)} + \text{Iron salt weight (mg)}} \times 100\% \qquad (1)$$

The iron salt weight corresponds to mass of the raw material: $FeCl_3$, $Fe_2(SO_4)_3$, $FeCl_2$, and $FeSO_4 \cdot 7H_2O$, respectively.

Physicochemical properties characterization of FG-iron nanocomposites. *Total sugar, carbon and protein contents determination.* Total sugar content in FG and FG-iron nanocomposites was determined using the simple phenol sulfuric acid colorimetric method.[32] Protein and total organic carbon contents in FG and FG-iron nanocomposites were determined by combustion analyses (CN628, LECO Corporation, St. Joseph, MI, USA) using methodologies suggested by Sweeney, et al., 1987 and Wright et al., 2001.[33,34] Protein content was estimated by multiplying the nitrogen content by a factor of 6.25.[35]

185 *Fourier transform infrared (FTIR) analysis.* FTIR spectroscopy was applied to investigate the
186 vibrations of molecules and polar bonds between the different atoms. Infrared spectrum analysis was
187 performed using a FTS-40 IR spectrometer (Bio-Rad Laboratories, Inc., Hercules, CA, USA). Five
188 milligrams of FG and 5 mg FG-iron nanocomposites were, individually, mixed with 200 mg potassium
189 bromide (KBr) and pelleted, prior to analysis. The FTIR spectra were recorded in the mid-IR region (4000–
190 400 cm^{-1} wavelength).

191 *Thermodynamic analysis.* Thermodynamic analysis was completed by heating a small subsample of FG
192 and synthetic FG-iron nanocomposites (8–12 mg) in aluminum pans from 25 to 500 °C at 10 °C/min under a
193 high purity nitrogen flow of 20 mL/min in order to avoid violent oxidation.[36] The resulting differential
194 scanning calorimetry (DSC) thermograms of FG and the synthetic FG-iron nanocomposites were recorded
195 on a Mettler DSC-1 system (ME-51140313, Mettler Toledo, China).

196 *X-ray powder diffraction (XRD).* X-ray diffraction patterns were obtained on FG and the FG-iron
197 nanocomposites samples using a CuK-α radiation and MiniFlex 300/600 diffraction system (Beijing Persee
198 General Instrument Co. Ltd.) equipped with a graphite monochromator. The samples were prepared by
199 spreading an even and thin layer of FG and FG-iron nanocomposites on each quartz slide prior to scanning.
200 Scans were made from 10° to 80° 2θ at 5°/min at 40 kV and 15 mA.[37]

201 *Micromorphology analysis*. Micromorphology of flaxseed, FG, and FG-iron nanocomposites were
202 investigated using a field emission scanning electron microscopy (FESEM, Ultra 55, Zeiss, Germany).
203 Samples were fixed on a small copper table and then sputter-coated with 20–30 nm gold powder, under
204 vacuum. Flaxseed, FG and FG-iron nanocomposites were captured on micrographs obtained on a FESEM
205 with 20, 100 and 5000-fold magnification, respectively, at 5.0 kV accelerated voltage.

206 *Particle size and zeta potential analysis.* Particle size distribution, z-average diameter (D*z*) and zeta
207 potential of FG-iron nanocomposites were evaluated using dynamic light scattering (DLS).[38] Samples were

mixed in absolute ethanol with a concentration of 0.1% (*w*/*v*) and immediately transferred into the quartz cuvette for size (D*z* and particle size distribution) and zeta potential determination. DLS analysis was performed at a fixed scattering angle of 173° using a Zetasizer Nano-ZS instrument (Malvern Instruments, Worcestershire, U.K.) equipped with a 4 mW He/Ne laser (λ = 633 nm) at 25 ± 0.1 °C.

***In vitro* release kinetics study of FG-iron nanocomposites.** The release characteristics of iron from the synthetic FG-iron nanocomposites were studied in SGF at 37 °C using a dialysis membrane as suggested by Katuwavila, et al., 2016 with minor modifications.[39] Briefly, 100 mg FG-iron nanocomposites were moistened with two drops of absolute ethanol, vortex mixed for 2 min in 10 mL SGF, and injected inside a dialysis membrane with a molecular weight cutoff of 3500 Da. The dialysis membrane was then immersed in 200 mL SGF at 37 °C for 5 h, with mild agitation, to simulate *in vitro* digestion. During the incubation, 1.0 mL aliquots of the dialyzate were withdrawn from outside of the dialysis membrane at predetermined time intervals and the iron release amounts were quantified and the cumulative release percentages were determined (See section *Quantification of iron content*).

To evaluate the kinetics of the drug release from a delivery system, the release profiles of iron from the FG-iron nanocomposites were fitted to five different mathematical models: Zero-order, First-order, Higuchi, Hixson-Crowell, and Korsemeyer-Peppas.[39–41] The model that exhibited the adjusted R^2 closest to unity (highest R^2 value) was selected as the best fit. The functions of the models with minor modifications are given as follows:

Zero-order model: $M_t/M_\infty = C_0+k_0t$ (2)

First-order model: $\log M_t/M_\infty = k_1t/2.303+C_1$ (3)

Higuchi model: $M_t/M_\infty = k_Ht^{1/2}+C_H$ (4)

Hixson-Crowell model: $(M_t/M_\infty)^{1/3} = k_{HC}t +C_{HC}$ (5)

Korsmeyer-Peppas model: $M_t/M_\infty = k_{KP}t^n$ (6)

Where M_t/M_∞ is the fraction of iron released at time t, k_0, k_1, k_H, k_{HC}, and k_{KP} are release rate constants of corresponding kinetic models, n is release exponent of Korsmeyer-Peppas model, t is time.

Data analysis. All experiments were carried out in triplicate. Data and graphic processing were performed in Microsoft Excel 2016 and Origin 9.0. Statistical analysis was analyzed using the unpaired Student's *t*-test ($n = 3$), and the values were presented as the means ± standard deviation (SD). The threshold for statistical significance was set at $p < 0.05$. Where applicable, the double standard deviations are shown as error bars around the mean value.

RESULTS AND DISCUSSION

Extraction of FG. FG was extracted from flaxseed hull with a yield of 11.92% of the hull mass (3.42% of seed weight) after lyophilization. The yield of FG varied with culture environment, crop age, genotype, and extraction conditions. Kaushik, et al., 2017 reported that the yield of FG increased from 2.1% to 8.4% (of seed weight) with increasing extraction temperature from 30 to 90 °C.[27] However, the purity of the gum decreased with the increasing extraction temperature. The freeze-dried FG was white with light reddish-brown and in a state of packed and crosslinked flakes. The main components of FG were carbohydrate and protein: 75.09±3.29% and 19.72±0.03% (*w*/*w*, $n = 3$), respectively (Table 1). These components can act as potential favourable recipient for iron ions. Furthermore, FG is readily dissolved in water, and thus can ensure successful development for an iron supplement. The value of FG yield, carbohydrate and protein content are similar to that reported by Roulard, et al., 2016 and Fatma, et al., 2016.[42,43]

Structure characterization of FG. *Monosaccharide composition.* Polysaccharides were the most abundant component in FG (Table 1). Gas chromatographic separation of FG identified rhamnose (33.73%), arabinose (24.35%), xylose (14.23%), glucose (4.54%), and galactose (23.15%) to be the dominant monosaccharides found in FG of this cultivar (CDC Sorrel) (Fig. 1B). However, monosaccharide

254 composition can vary with flax cultivated varieties, growth environment, growth period and harvest time.[44]
255 For instance, Oomah et al., 1995 reported the xylose percentage ranging from 10.9% to 32.0% among
256 different water-soluble flaxseed polysaccharides from twelve geographical regions flax.[44]

257 *NMR analysis.* NMR can provide detailed structural information, including the monosaccharide
258 composition, α- or β-anomeric configurations, linkage patterns, and sequences of the sugar units.[45] Therefore,
259 the ^{13}C and ^{1}H NMR were conducted to investigate the possible linkage types and anomeric configurations
260 of the polysaccharides found in FG. In the ^{13}C-NMR (Fig. 1C), chemical shift resonances at 99.36 ppm (C1)
261 and 77.74 ppm (C4) can be attributed to the →4)-β-D-Xyl*p*-(1→ residue.[46] The presence of weak peaks at
262 173.6–174.5 ppm and signals at 70.05, 69.69, 68.36 ppm are evidence of →4)-α-D-Gal*p*A-(1→, residues
263 while resonances at 17.11 and 16.02 probably originated from the residues of →2)-α-L-Rha*p*-(1→ and
264 T-α-L-Fuc*p*-(1→, respectively.[47] The chemical shift of 71.34−77.18 ppm were attributed to the C-2, C-3,
265 C-4, C-5 epimers.[48] C-6 resonances typically are located from 60−64 ppm, however, after substitution these
266 resonances were shifted between 67 and 70 ppm.[48,49] Resonances at 103.80, 74.15, 70.05, and 17.1 ppm
267 were also attributed to →2)-α-L-Rha*p*-(1→. Unfortunately, due to the high molecular weight and solution
268 viscosity of the gum, the ^{13}C-NMR has weak resonance and poor resolution, which provided limited
269 structural details.

270 Signals at 5.03, 5.08 and 5.13 ppm, from the ^{1}H-NMR spectrum, were assigned to the H-1 of
271 →1)-α-L-Ara*f*-(5→, →1)-α-L-Ara*f*-(3,5→ and T-α-L- Ara*f*-(1→, respectively (Figs. 1D, 1E).[50] In addition,
272 the ^{1}H-NMR spectrum revealed five primary linkage patterns at δ 4.07, 3.92, 3.84, 3.77, 3.90, indicating that
273 the carbon atoms were mainly in the β-configuration.[51] Signals ranging between 4.7 and 4.3 ppm were
274 assigned to the anomeric proton of galactose and glucose residues, which were →1)-β-D-Gal*p*-(2→,
275 T-β-D-Gal*p*-(1→, → 1-β-D-Glu*p*-(4→, and →1-β-D-Glu*p*-(4,6→, respectively.[52] The resonance at 1.29 ppm
276 was assigned to the H-6 of →1)-α-L-Rha*p*-(2→ or →1)-α-L-Rha*p*-(2,4→.[47] Altogether, the monosaccharide

277 composition and NMR analyses suggest that the backbone structures of FG polysaccharide are similar to
278 what was previously reported:[47,50,52] →2)-α-L-Rha*p*-(1→4)-α-D-Gal*p*-(1→ and
279 →4)-β-D-Xyl*p*-(1→3,5)-α-L-Ara*f* -(1→2)-α-D-Xyl*p*-(1→ with highly monobranched sugar residues
280 including T-α-D-Ara*f*-(1→, T-α-D-Xyl*p*-(1→, T-α-L-Fuc*p*-(1→ and T-β-D-Gal*p*-(1→. This result is
281 consistent with previous literatures that reported FG polysaccharides consist of neutral fraction
282 arabinoxylans and acidic fraction rhamnogalacturonans.[20,21] However, purification of the compound and
283 2D-NMR spectroscopy should be conducted for further confirmation of the structural details of FG
284 polysaccharides.

285 **Synthesis of FG-iron nanocomposites.** FG comprising of heteropolysaccharides and proteins was
286 considered as a favourable potential ligand for iron ions. In this study, FG was transformed into Fe (III)- and
287 Fe (II)-form *via* ion-exchange against $FeCl_3$, $Fe_2(SO4)_3$, $FeCl_2$, and $FeSO_4 \cdot 7H_2O$, respectively. Optimum
288 reaction conditions were screened according to the iron content and product yields (Fig. 2). Of the four
289 tested chelated complexes, FG-$FeCl_3$ and FG-$FeSO4 \cdot 7H_2O$ showed high iron loading contents, indicative of
290 an increased binding ability for iron ions. However, most of iron in the FG-$FeSO_4 \cdot 7H_2O$ complex are in the
291 free state, and thus had minimal delayed release. This could potentially contribute to an increase in side
292 effects similarly found in free ferrous supplements. Therefore, Fe^{2+} from $FeSO_4 \cdot 7H_2O$, although can be
293 combined with FG, will not bind tightly, thus is freely released when dissolved in water. On the contrary, the
294 iron in the FG-$FeCl_3$ complex is largely found in the bound state (> 95%). This suggests that the FG-$FeCl_3$
295 complex is potentially an excellent vehicle as an iron supplement and exhibits minimal side effects for
296 potential treatment of IDA or other related diseases. It is corresponded to the reported researches which
297 acquiescently applied $FeCl_3$ as the iron source for the synthesis of polysaccharide and iron complexes.[17,53]
298 Finally, iron content in the FG-$Fe_2(SO_4)_3$ and FG-$FeCl_2$ complexes were relatively low compared with
299 FG-$FeCl_3$ and FG-$FeSO_4 \cdot 7H_2O$ complexes. Fortunately, the iron in these two complexes were always found

to be in the bound state. In summary, of the four tested chelated complexes, FG-$FeCl_3$ demonstrated the best binding affinity.

Temperature played a significant role in the binding of iron to FG, with elevated temperatures favouring this binding process (Figs. 2Aa, 2Ba). For example, total iron content in FG-$FeSO_4 \cdot 7H_2O$ complexes were 20.82%, 22.89%, and 30.26% at temperatures of 20, 50, and 80 °C, respectively (Fig. 2Aa). The product yields of FG-$Fe_2(SO_4)_3$ complexes were 37.64%, 40.39%, and 43.24% at temperatures of 20, 50, and 80 °C, respectively (Fig. 2Ba). However, FG-$FeCl_3$ was an exception where $FeCl_3$ was continuously bound to FG at all three temperature gradients. The ratio of iron to FG (I:G) illustrated that the iron loading contents increased proportionally to the amount of iron present (Fig. 2Ab). This indicated that the FG was not overloaded with iron at the amounts studied. However, the product yields were inversely correlated with the iron proportion except for the FG-$FeSO_4 \cdot 7H_2O$ complex (Fig. 2Bb). Alternatively, a ratio of 1:2 for I:G was chosen, as high iron content is preferred to adequate binding affinity with the FG. Interestingly, reaction time played an insignificant role, compared to temperature and I:G, in the loading capabilities and binding affinities among the iron and FG (Fig. 2Ac). The product yields were also irrelevant to reaction time except for the FG-$FeSO_4 \cdot 7H_2O$ complex (negatively correlated) (Fig. 2Bc). However, for fully chelation between FG and iron, 2 h is preferred rather than 1 h. Taken altogether, the most favourable conditions contributing to overall iron-binding capabilities and product yield for the synthesis of FG-iron complexes included: a reaction temperature of 80 °C, 1:2 ratio of I:G (*w*:*w*, in which I is the iron's mass), and a reaction time of 2 h.

The expanded pilot study. The FG-iron nanocomposites consisted primarily of carbohydrates, proteins and sugars (Table 1). Interestingly, total sugar and protein content observed an overall decrease in the presence of iron. However, the relative ratio between carbohydrates and proteins remained relatively constant. Based on the screened reaction conditions in the above experiments, an expanded study was

performed to prepare sufficient samples for further study. The product yields, iron content and compound composition of the synthetic nanocomposites were recorded (Table 1). The yields of FG-$FeCl_3$, FG-$Fe_2(SO_4)_3$, FG-$FeCl_2$, and FG-$FeSO_4 \cdot 7H_2O$ complexes were 48.56%, 42.32%, 38.39%, and 56.08%, respectively, which are consistent with the results from the initial screening experiments. The total iron content in these four complexes were 25.51%, 10.36%, 5.83%, and 22.83%, in which combined iron content represented 24.96%, 8.55%, 3.92%, and 8.27%, respectively. Most of the iron were observed in the bound state (FG-$FeCl_3$, 97.84%; FG-$Fe_2(SO_4)_3$, 82.53%; FG-$FeCl_2$, 67.24%) except for the FG-$FeSO_4 \cdot 7H_2O$ complexes whose iron were mostly in the free state (63.73%). The valence electron of iron is also an important evaluation indicator because it is closely related to absorption efficiency. Seen from table 1, ferric and ferrous iron coexist in the nanocomposites, and most of the iron were in the same valence as the original iron salts except for FG-$FeCl_2$ nanocomposites whose iron were mostly found in the ferric state (73.93%) (Table 1). This suggests that the ferrous iron is almost completely oxidized during the reaction process, possibly due to the loss of protection from FG.

Qualitative identification of the nanocomposites. A simple colorimetric assay using KSCN (for Fe^{3+} detection) and 1,10-phenanthroline (for Fe^{2+} detection) was utilized to observe the efficient removal of free iron ions from the FG-iron complexes (Fig. 3A). This simple assay confirms that most of the iron salts can be completely dissolved in anhydrous ethanol ($FeCl_3$, $Fe_2(SO_4)_3$) or 80% ethanol ($FeCl_2$), while precipitating the FG and FG-iron nanocomposites. As a result, free irons were removed and the combined irons (ferric and ferrous) remained bound in the FG. The one exception was the $FeSO_4 \cdot 7H_2O$ nanocomposite, where poorer solubility in anhydrous ethanol and 80% ethanol was observed. Furthermore, when the iron salts were dissolved in deionized water, $FeSO_4 \cdot 7H_2O$ was the only sample to exhibit noticeable free iron ions in the solution, whereas the other three iron salts retained the iron in the bound state (see colour change in Fig. 3B; first panel). Regardless, these four nanocomposites exhibited poor solubility in deionized water (i.e. the

samples were in a suspended state). However, when dissolved in 1 M HCl for 24 h, these complexes were totally broken and released free iron into the acidic environment. This demonstrates that these nanocomposites are effective in maintaining iron in a bound state (except for the FG-$FeSO_4 \cdot 7H_2O$ complex), until in the presence of an acidic environment, such as gastric fluid in the stomach (Fig 3B), where it is slowly released.

Structure characterization of FG-nanocomposites. *FTIR analysis.* Infrared spectroscopy was utilized in this study to investigate the binding interaction between iron ions and the polysaccharide from FG. FTIR analysis was performed on a FTS-40 IR spectrometer and results are illustrated in Fig. 4A. As expected, FG showed typical characteristic absorption bands of a polysaccharide (Fig. 4Aa), in which the main absorptions occurred at wavenumbers: 3424.42 cm^{-1} (O-H), 2929.29 cm^{-1} (-CH_2-), 1651.18 cm^{-1} (C=O), 1534.86 cm^{-1} (amide II band, assigned to protein), 1414.65 cm^{-1} (C-OH), 1040.59 cm^{-1} (C-O-H and C-O-C), 896.26 cm^{-1} (C-H deformation vibration in β-isomer of D-pyranose), and 630.42 cm^{-1} (C-H).[54,55] Likewise, FG-$FeCl_3$, FG-$Fe_2(SO_4)_3$, and FG-$FeCl_2$ nanocomposites illustrated similar IR spectra to that of FG (Fig 4Ab, c, d), although there were some subtle differences. Firstly, the band of the stretching vibrations of the hydroxyl groups (3424.42 cm^{-1}) became broader and shifted towards a lower wavenumber (3370 cm^{-1}, 3394 cm^{-1}, and 3404 cm^{-1}, respectively), suggesting an enhanced hydrogen bond interaction that may be caused by the formation of the iron core or interaction between the iron core and FG polysaccharide.[36] Secondly, the presence of bands of C=O asymmetric stretching vibrations (1734.70, 1735.09, and 1736.12 cm^{-1}) are indicative of an interaction involving the carboxylate groups and its complexation to iron. Thirdly, significant changes in the spectra of the iron loading nanocomposites were observed at wavenumbers 473.95 cm^{-1} (FG-$FeCl_3$), 508.92 and 475.16 cm^{-1} (FG-$Fe_2(SO_4)_3$), and 506.34 cm^{-1} (FG-$FeCl_2$). The formation of a broad shoulder, appearing in this 570–438 cm^{-1} region, can be attributed to the presence of iron oxides (Fe-O), indicating the formation of an iron core in the nanocomposites.[56,57] The minor differences of the IR

spectra between FG and the nanocomposites indicated that the reactions between FG and the iron ions were close chemical chelation instead of simple physical mixture. As an exception, the IR spectra of FG-$FeSO_4 \cdot 7H_2O$ nanocomposite (Fig. 4Ae) is quite different from the FG spectra and the other three nanocomposites, which exhibits both characteristic absorptions of polysaccharide and $FeSO_4 \cdot 7H_2O$, suggesting poorer complexation between FG and $FeSO_4 \cdot 7H_2O$.

DSC analysis. DSC analyses demonstrated that the synthetic nanocomposites exhibited similar thermal stability as FG. The DSC thermograms revealed an endothermic peak occurring at around 160 °C and an exothermic peak at around 272 °C in FG (Fig. 4Ba). The endothermic peak represents the heat required to break various intra and intermolecular hydrogen bonding within the polymeric matrix (e.g. melting), and the exothermic peak is related to polymeric degradation (e.g. oxidation).[58] For the synthetic nanocomposites: FG-$FeCl_3$, FG-$Fe_2(SO_4)_3$, FG-$FeCl_2$, and FG-$FeSO_4 \cdot 7H_2O$ nanocomposites, the first major endothermic peaks occurred at 121 °C, 199 °C, 116 °C, and 156 °C (the initial minor peak for the FG-$FeSO_4 \cdot 7H_2O$ nanocomposite corresponds to evaporation of water; Fig. 4Be), respectively. These endothermic peaks demonstrate that the structures of intra and intermolecular hydrogen bonding were changed by the induction of iron ions. Interestingly, the FG-$FeSO_4 \cdot 7H_2O$ nanocomposite, was the only complex to exhibit a second major endothermic peak at 343 °C, suggesting that the chelation processes were inefficient in retaining the iron ions. Meanwhile, there were less obvious exothermic peaks at increased temperatures, suggesting increased thermal stability and minimal degradation of the nanocomposites.

XRD analysis. XRD pattern analyses identified characteristic differences among FG and the synthetic nanocomposites (Fig. 4C). The broad peak ($2\theta = 21.6°$) observed in the XRD pattern of FG, indicates that FG is an amorphous substance (Fig. 4Ca). Patterns of FG-$FeCl_3$ and FG-$Fe_2(SO_4)_3$ nanocomposites exhibit three distinct sharp absorption peaks occurring at 19.9°, 21.1°, and 29.3°, suggesting the presence of new compounds or complexes forming during the reaction between FG and $FeCl_3$ and $Fe_2(SO_4)_3$ (Fig. 4Cb, c).

Meanwhile, the FG-$FeCl_2$ nanocomposite exhibited a similar pattern as FG, due to the low iron content (Fig. 4Cd). Finally, the FG-$FeSO_4 \cdot 7H_2O$ nanocomposite illustrated the most distinct and fairly complex XRD pattern (Fig. 4Ce). The abundance of peaks corresponds to the presence of many complicated iron compounds. These patterns of the nanocomposites could be representative of hematite (α-Fe_2O_3), magnetite (Fe_3O_4), goethite (α-FeOOH), and ferrihydrite ($Fe_2O_3 \cdot nH_2O$).[16] This demonstrates that hydroxyl or carboxyl groups in FG polysaccharide plays a critical role in the complexation between iron and FG, therefore providing oxygen and hydrogen atoms for further formation of stable iron compound crystals.

Scanning electron microscopy characterization. FESEM was performed to study the micromorphology of the synthetic nanocomposites and raw materials (flaxseed and FG). Flaxseed is a sesame-like fusiformis seed with macro-axis and minor-axis values of 4.5 and 2.1 mm, respectively; while FG is in the state of inerratic sheet stacking (Fig. 5A). FESEM imagery revealed that the synthetic nanocomposites conglomerated in shapes of irregular granules and lumps (Fig. 5A). However, FG-$FeCl_3$ and FG-$Fe_2(SO_4)_3$ nanocomposites exhibited more uniformity than the FG-$FeCl_2$ and FG-$FeSO_4 \cdot 7H_2O$ nanocomposites (Fig. 5A). This is possibly due to the changes in the processing methods (e.g. drying and grinding) or differences between the ferric and ferrous irons.

Particle size and zeta potential analysis. Particle size and zeta potential analyses were conducted on a Zetasizer Nano-ZS instrument. Seen from Fig. 5B, particle size distribution of these synthetic composites were on the nanoscale level (100–1000 nm) and conform to normal distribution model. Dz of FG-$FeCl_3$, FG-$Fe_2(SO_4)_3$, FG-$FeCl_2$, and FG-$FeSO_4 \cdot 7H_2O$ are 808.6, 843.4, 664.2, and 588.1 nm, respectively. Thus, these synthetic composites can be classified as "nanoparticles", which defined as particulate dispersions or solid particles with a size in the range of 10–1000 nm.[59] Meanwhile, zeta potential was evaluated to investigate the stability of the synthetic nanocomposites in ethanol dispersion system. The FG-$FeCl_3$ complex exhibited the highest stability with a zeta potential of –26.7 mV. The remaining FG-$Fe_2(SO_4)_3$,

FG-$FeCl_2$, and FG-$FeSO_4 \cdot 7H_2O$ nanocomposites, had zeta potentials of –6.51, –17.2, and –14.3 mV, respectively, indicating relatively poor stability.

***In vitro* release kinetics of FG-iron nanocomposites.** Stomach acid or gastric juice are detrimental for the digestion of most nutrients, especially acid sensitive substances, prior to their adsorption in the gut. Therefore, it is important to investigate the *in vitro* release kinetics, mechanisms and effects of iron, from these nanocomposites, within a similar acidic environment. It is an important and essential part before simulating intestinal digestion. The release profiles of iron from the nanocomposites demonstrated the effective delayed iron release in response to SGF (Fig. 6), compared with the original iron salts. For example, the cumulative iron release of FG-$FeCl_3$ nanocomposite and $FeCl_3$ at 3.0 h were 34.53% and 82.11%, respectively. This iron delay property suggests that these iron binding nanocomposites could be potentially developed as novel iron supplements with minimal side effects for treatment of IDA and other related diseases. After 5 h simulated digestion in SGF, the cumulative release amount of iron from FG-$FeCl_3$, FG-$Fe_2(SO_4)_3$, FG-$FeCl_2$, and FG-$FeSO_4 \cdot 7H_2O$ nanocomposites were 56.99%, 55.90%, 68.64%, and 68.93%, respectively. It appears that the binding effects of FG on ferric iron are better than ferrous iron when in the presence of a SGF environment. This is consistent with the determined iron content for these four nanocomposites, detailed in Table 1.

It appears that the iron release kinetics of the nanocomposites, as well as the original iron salts $FeCl_3$ and $Fe_2(SO_4)_3$, closely supported the Korsmeyer-Peppas model more so than the other kinetics models (R^2 values ranging between 0.8384 and 0.9827, Table 2). Korsmeyer-Peppas model proposed a semi-empirical design in which the drug release is proportional to the sum of two different powers of time which account for the pure diffusivity contribution.[39] In this kinetic model, the release exponent "*n*" is an important indicator of the mechanism of the drug release from the nanocomposites. For spherical particles, $n \leq 0.43$ indicates a Fickian diffusion, while $0.43 < n < 0.85$, indicates a non-Fickian release (an anomalous transport

behavior), and $n \geq 0.85$ represent Case II transport mechanism.[60] Therefore, the iron release mechanism from FG-$FeCl_3$ was determined to be *via* a Case II transport mechanism (n = 1.6808), while the other three nanocomposites, as well as $FeCl_3$ and $Fe_2(SO_4)_3$ release mechanisms, suggested non-Fickian anomalous diffusion processes (n-values ranging between 0.4377 and 0.6370, Table 2). Meanwhile, the original iron salts $FeCl_2$ and $FeSO_4 \cdot 7H_2O$, followed the Higuchi model with R^2 value of 0.9735 and 0.9809, respectively. This model describes the drug release as liquid penetration followed by drug diffusion into the exterior solution depending on the concentration gradient.[41] The *in vitro* release experiments proved that the synthetic nanocomposites are effective for delaying iron release in SGF. From a physiological point of view, in the future study, cell culture techniques are needed for further evaluating iron bioavailability of the nanocomposites.

AUTHOR INFORMATION

Corresponding author

* Tel: +86-020-85220032. Fax: +86-020-85226630. E-mail: twyong@jnu.edu.cn.

Acknowledgement

The authors would like to thank Dr Jianheng Shen and Dr Timothy Tse for their technical assistances and altruistic supports.

Funding

The financial support from National Key Research and Development Program of China under grant 2017YFD0400200, and the Department of Science and Technology of Guangdong Province under grants 2017B090907018, 2016A010105010 and 2017A030310012 are gratefully acknowledged.

Notes

The authors declare no competing financial interest.

REFERENCES

(1) Tang, M.; Wang, D.; Hou, Y.; Buchili, P.; Sun, L., Preparation, characterization, bioavailability *in vitro* and *in vivo* of tea polysaccharides–iron complex. *Eur. Food Res. Technol.* **2012**, *236*, 341–350.

(2) Ward, R. J.; Crichton, R. R., Iron: Properties and Determination. In *Encyclopedia of Food and Health*, Academic Press: Oxford, United Kingdom, **2016**; pp. 468–475.

(3) Somsook, E.; Hinsin, D.; Buakhrong, P.; Teanchai, R.; Mophan, N.; Pohmakotr, M.; Shiowatana, J., Interactions between iron(III) and sucrose, dextran, or starch in complexes. *Carbohydr. Polym.* **2005**, *61*, 281–287.

(4) Umbreit, J., Iron deficiency: A concise review. *Am. J. Hematol.* **2005**, *78*, 225–231.

(5) von Haehling, S.; Jankowska, E. A.; van Veldhuisen, D. J.; Ponikowski, P.; Anker, S. D., Iron deficiency and cardiovascular disease. *Nat. Rev. Cardiol.* **2015**, *12*, 659–69.

(6) Lundqvist, H.; Sjöberg, F., Food interaction of oral uptake of iron/a clinical trial using ^{59}Fe.

Arzneim.-Forsch. **2007**, *57*, 401–416.

(7) Tapiero, H.; Gaté, L.; Tew, K. D., Iron: deficiencies and requirements. *Biomed. & Pharmacother.* **2001**, *55*, 324–332.

(8) Camaschella, C., New insights into iron deficiency and iron deficiency anemia. *Blood Rev.* **2017**, *31*, 225–233.

(9) Macdougall, I. C., Strategies for iron supplementation: Oral versus intravenous. *Kidney Int.* **1999**, *55*, S61–S66.

(10) Fairbanks, V. F.; Fahey, J. L.; Beutler, E., *Clinical disorders of iron metabolism*, 2nd ed.; Grune & Stratton: Rolando, Florida, **1971**.

(11) Pritchard, J. A., Hemoglobin regeneration in severe iron-deficiency anemia. Response to orally and parenterally administered iron preparations. *Jama-J. Am. Med. Assoc.* **1966**, *195*, 717–720.

(12) Zhang, X.; Ouyang, J.; Wieczorek, R.; DeSoto, F., Iron medication-induced gastric mucosal injury. *Pathol. Res. Pract.* **2009**, *205*, 579–581.

(13) Koskenkorva-Frank, T. S.; Weiss, G.; Koppenol, W. H.; Burckhardt, S., The complex interplay of iron metabolism, reactive oxygen species, and reactive nitrogen species: Insights into the potential of various iron therapies to induce oxidative and nitrosative stress. *Free Radical Biol. Med.* **2013**, *65*, 1174–1194.

(14) Wang, J.; Chen, H.; Wang, Y.; Xing, L., Synthesis and characterization of a new Inonotus obliquus polysaccharide-iron(III) complex. *Int. J. Biol. Macromol.* **2015**, *75*, 210–217.

(15) Pitarresi, G.; Tripodo, G.; Cavallaro, G.; Palumbo, F. S.; Giammona, G., Inulin-iron complexes: a potential treatment of iron deficiency anaemia. *Eur. J. Pharm. Biopharm.* **2008**, *68*, 267–276.

(16) Coe, E. M.; Bowen, L. H.; Bereman, R. D.; Speer, J. A.; Monte, W. T.; Scaggs, L., A study of an iron dextran complex by Mössbauer spectroscopy and x-ray diffraction. *J. Inorg. Biochem.* **1995**, *57*, 63–71.

(17) Lu, Q.; Xu, L.; Meng, Y.; Liu, Y.; Li, J.; Zu, Y.; Zhu, M., Preparation and characterization of a novel

Astragalus membranaceus polysaccharide-iron (III) complex. *Int. J. Biological Macromolecules* **2016**, *93*, 208–216.

(18) F Sanders, J., Clinical response to iron-polysaccharide complex in geriatric patients with iron-deficiency anemia. *Mich. Med.* **1968**, *67*, 726–727.

(19) Debon, S. J. J.; Tester, R. F., *In vitro* binding of calcium, iron and zinc by non-starch polysaccharides. *Food Chem.* **2001**, *73*, 401–410.

(20) Ding, H. H.; Qian, K.; Goff, H. D.; Wang, Q.; Cui, S. W., Structural and conformational characterization of arabinoxylans from flaxseed mucilage. *Food Chem.* **2018**, *254*, 266–271.

(21) Elboutachfaiti, R.; Delattre, C.; Quéro, A.; Roulard, R.; Duchêne, J.; Mesnard, F.; Petit, E., Fractionation and structural characterization of six purified rhamnogalacturonans type I from flaxseed mucilage. *Food Hydrocolloids* **2017**, *62*, 273–279.

(22) Liu, J.; Shim, Y. Y.; Poth, A. G.; Reaney, M. J. T., Conlinin in flaxseed (*Linum usitatissimum* L.) gum and its contribution to emulsification properties. *Food Hydrocolloids* **2016**, *52*, 963–971.

(23) Liu, J.; Shim, Y. Y.; Shen, J.; Wang, Y.; Ghosh, S.; Reaney, M. J. T., Variation of composition and functional properties of gum from six Canadian flaxseed (Linum usitatissimum L.) cultivars. *Int. J. Food Sci. Technol.* **2016**, *51*, 2313–2326.

(24) Darzi, H. H.; Larimi, S. G.; Darzi, G. N., Synthesis, characterization and physical properties of a novel xanthan gum/polypyrrole nanocomposite. *Synth. Met.* **2012**, *162*, 236–239.

(25) Hajji, S.; Salem, S. B.; Hamdi, M.; Jellouli, K.; Ayadi, W.; Nasri, M.; Boufi, S., Nanocomposite films based on chitosan–poly(vinyl alcohol) and silver nanoparticles with high antibacterial and antioxidant activities. *Process Saf. Environ. Prot.* **2017**, *111,* 112–121.

(26) Wang, L. F.; Rhim, J. W., Functionalization of halloysite nanotubes for the preparation of carboxymethyl cellulose-based nanocomposite films. *Appl. Clay Sci.* **2017**, *150*, 138–146.

(27) Kaushik, P.; Dowling, K.; Adhikari, R.; Barrow, C. J.; Adhikari, B., Effect of extraction temperature on composition, structure and functional properties of flaxseed gum. *Food Chem.* **2017**, *215*, 333–340.

(28) Chen, Y.; Xie, M. Y.; Nie, S. P.; Li, C.; Wang, Y. X., Purification, composition analysis and antioxidant activity of a polysaccharide from the fruiting bodies of Ganoderma atrum. *Food Chem.* **2008**, *107*, 231–241.

(29) Liang, S.; Liao, W.; Ma, X.; Li, X.; Wang, Y., H_2O_2 oxidative preparation, characterization and antiradical activity of a novel oligosaccharide derived from flaxseed gum. *Food Chem.* **2017**, *230*, 135–144.

(30) Loeppert, R. L.; Inskeep, W. P., *Colorimetric determination of ferrous iron and ferric iron by the 1,10-phenanthroline method*. SSSA: Madison, Wisconsin, **1996**; pp. 659–661.

(31) Schefer, L.; Bulant, A.; Zeder, C.; Saha, A.; Mezzenga, R., Magnetic Control of Macromolecular Conformations in Supramolecular Anionic Polysaccharide–Iron Complexes. *Angew. Chem. Int. Ed.* **2015**, *54*, 13289–13292.

(32) DuBois, M.; Gilles K. A, E.; Hamilton, J. K.; A. J. Rebers, P.; Smith, F., Calorimetric Dubois Method for Determination of Sugar and Related Substances. *Anal. Chem*. **2002**, *28*, 350–356.

(33) Sweeney, R. A.; Rexroad, P. R., Comparison of LECO FP-228 "nitrogen determinator" with AOAC copper catalyst Kjeldahl method for crude protein. *J. Assoc. Off. Anal. Chem.* **1987**, *70*, 1028–1030.

(34) Wright, A. F.; Bailey, J. S., Organic carbon, total carbon, and total nitrogen determinations in soils of variable calcium carbonate contents using a Leco CN-2000 dry combustion analyzer. *Commun. Soil Sci. Plant Anal.* **2001**, *32*, 3243–3258.

(35) Sosulski, F. W.; Imafidon, G. I., Amino acid composition and nitrogen-to-protein conversion factors for animal and plant foods. *J. Agric. Food Chem.* **1990**, *38*, 1351–1356.

(36) Wang, K. P.; Chen, Z. X.; Zhang, Y.; Wang, P. P.; Wang, J. H.; Dai, L. Q., Molecular Weight and Proposed Structure of the Angelica sinensis Polysaccharide-iron Complex. *Chin. J. Chem.* **2008**, *26*, 1068–1074.

553 (37) Coe, E. M.; Bowen, L. H.; Speer, J. A.; Bereman, R. D., Comparison of polysaccharide iron complexes
554 used as iron supplements. *J. Inorg. Biochem.* **1995**, *57*, 287–292.
555 (38) Tan, C.; Xie, J.; Zhang, X.; Cai, J.; Xia, S., Polysaccharide-based nanoparticles by chitosan and gum
556 arabic polyelectrolyte complexation as carriers for curcumin. *Food Hydrocolloids* **2016**, *57*, 236–245.
557 (39) Katuwavila, N. P.; Perera, A. D. L. C.; Dahanayake, D.; Karunaratne, V.; Amaratunga, G. A. J.;
558 Karunaratne, D. N., Alginate nanoparticles protect ferrous from oxidation: Potential iron delivery system. *Int.*
559 *J. Pharm.* **2016**, *513*, 404–409.
560 (40) Lokhandwala, H.; Deshpande, A.; Deshpande, S., Kinetic modeling and dissolution profiles comparison:
561 An overview. *Int. J. Pharma. Biosci.* **2013**, *4*, 728–737.
562 (41) Singhvi, G.; Singh, M., *Review: In vitro* Drug Release Characterization Models. *Int. J. Pharm. Stud.*
563 *Res.***2011***, 2*, 77–84.
564 (42) Roulard, R.; Petit, E.; Mesnard, F.; Rhazi, L., Molecular investigations of flaxseed mucilage
565 polysaccharides. *Int. J. Biol. Macromol.* **2016**, *86*, 840–847.
566 (43) Bouaziz, F.; Koubaa, M.; Barba, F.; Roohinejad, S.; Chaabouni Ellouz, S., Antioxidant Properties of
567 Water-Soluble Gum from Flaxseed Hulls. *Antioxidants* **2016**, *5*, 26, 1–10.
568 (44) Oomah, B. D.; Kenaschuk, E. O.; Cui, W.; Mazza, G., Variation in the composition of water-soluble
569 polysaccharides in flaxseed. *J. Agric. Food Chem.* **1995**, *43*, 1484–1488.
570 (45) Li, J.; Fan, L.; Ding, S., Isolation, purification and structure of a new water-soluble polysaccharide from
571 *Zizyphus jujuba cv. Jinsixiaozao*. *Carbohydr. Polym.* **2011**, *83*, 477–482.
572 (46) Young, N. M.; Brisson, J.-R.; Kelly, J.; Watson, D. C.; Tessier, L.; Lanthier, P. H.; Jarrell, H. C.; Cadotte,
573 N.; Michael, F. S.; Aberg, E., Structure of the N-linked glycan present on multiple glycoproteins in the
574 Gram-negative bacterium, Campylobacter jejuni. *Campylobacter jejuni*. *J. Biol. Chem.* **2002**, *277*,
575 42530–42539.

576 (47) Qian, K.-Y.; Cui, S. W.; Nikiforuk, J.; Goff, H. D., Structural elucidation of rhamnogalacturonans from
577 flaxseed hulls. *Carbohydr. Res.* **2012,** *362*, 47–55.
578 (48) Cui, H.; Liu, Q.; Tao, Y.; Zhang, H.; Zhang, L.; Ding, K., Structure and chain conformation of a
579 (1→6)-α-d-glucan from the root of Pueraria lobata (Willd.) Ohwi and the antioxidant activity of its sulfated
580 derivative. *Carbohydr.Polym.* **2008,** *74*, 771–778.
581 (49) Daffe, M.; Brennan, P. J.; McNeil, M., Predominant structural features of the cell wall arabinogalactan
582 of *Mycobacterium tuberculosis* as revealed through characterization of oligoglycosyl alditol fragments by
583 gas chromatography/mass spectrometry and by ^{1}H and ^{13}C NMR analyses. *J. Biol. Chem.* **1990**, *265*,
584 6734–6743.
585 (50) Cordeiro, L. M. C.; Reinhardt, V. d. F.; Baggio, C. H.; Werner, M. F. d. P.; Burci, L. M.; Sassaki, G. L.;
586 Iacomini, M., Arabinan and arabinan-rich pectic polysaccharides from quinoa (*Chenopodium quinoa*) seeds:
587 Structure and gastroprotective activity. *Food Chem.* **2012**, *130*, 937–944.
588 (51) Ding, H. H.; Cui, S. W.; Goff, H. D.; Chen, J.; Wang, Q.; Han, N. F., Arabinan-rich
589 rhamnogalacturonan-I from flaxseed kernel cell wall. *Food Hydrocolloids* **2015**, *47*, 158–167.
590 (52) Ding, H. H.; Cui, S. W.; Goff, H. D.; Chen, J.; Guo, Q.; Wang, Q., Xyloglucans from flaxseed kernel
591 cell wall: Structural and conformational characterisation. *Carbohyd.Polym.* **2016,** *151*, 538–545.
592 (53) Gao, W.; Huang, Y.; He, R.; Zeng, X.-a., Synthesis and characterization of a new soluble soybean
593 polysaccharide-iron(III) complex using ion exchange column. *J. Biol. Macromol.* **2018**, *108*, 1242–1247.
594 (54) Chylińska, M.; Szymańska-Chargot, M.; Zdunek, A., FT-IR and FT-Raman characterization of
595 non-cellulosic polysaccharides fractions isolated from plant cell wall. *Carbohydr. Polym.* **2016**, *154*, 48–54.
596 (55) Nikolić, G.; Cakic, M., Physical investigation of the colloidal iron-inulin complex. *Colloid J.* **2007**, *69*,
597 464–473.
598 (56) Tonković, M.; Hadžija, O.; Nagy-Czako, I., Preparation and properties of Fe(III) sugar complexes.

Inorg. Chim. Acta **1983**, *80*, 251–254.

(57) Wei, C.; Nan, Z., Effects of experimental conditions on one-dimensional single-crystal nanostructure of β-FeOOH. *Mater. Chem. Phys.* **2011**, *127*, 220–226.

(58) AlKhatib, H. S.; Taha, M. O.; Aiedeh, K. M.; Bustanji, Y.; Sweileh, B., Synthesis and *in vitro* behavior of iron-crosslinked N-methyl and N-benzyl hydroxamated derivatives of alginic acid as controlled release carriers. *Eur. Polym. J.* **2006**, *42*, 2464–2474.

(59) Mohanraj, V. J.; Chen, Y., Nanoparticles - A review. *Trop. J. Pharm. Res.* **2006**, *5*, 561–573.

(60) Ritger, P. L.; Peppas, N. A., A simple equation for description of solute release II. Fickian and anomalous release from swellable devices. *J. Controlled Release* **1987**, *5*, 37–42.

Figure captions

Fig. 1 Gas chromatograms of monosaccharide compositions of (A) monosaccharide standards and (B) FG. NMR spectra of FG: (C) ^{13}C-NMR spectrum, (D) ^{1}H-NMR spectrum, (E) partial enlarged detail of ^{1}H-NMR spectrum.

Fig. 2 (A) Iron contents and (B) product yields of FG and iron loaded nanocomposites under different reaction conditions (FI: free iron; CI: combined iron). Data are represented as means and standard deviations (n = 3). Different letters on the top of columns represent significant difference of total iron at the $p < 0.05$ level.

622 **Fig. 3** Colorimetric assay for the removal of free iron ions. (A) Decreases of free iron during ethanol
623 precipitate (1st) and washing (2nd, 3rd, and 4th) procedures. (B) Products qualitative identification results (a,
624 dissolved in deionized water for 24 h; b, dissolved in 1 M HCl for 24 h). □, □, □, and □ refer to FG-$FeCl_3$,
625 FG-$Fe_2(SO_4)_3$, FG-$FeCl_2$, and FG-$FeSO_4 \cdot 7H_2O$ nanocomposites, respectively.
626 **Fig. 4** (A) FTIR spectra, (B) DSC thermograms, and (C) XRD patterns of FG and the synthetic iron loading
627 nanocomposites. a, FG; b, FG-$FeCl_3$; c, FG-$Fe_2(SO_4)_3$; d, FG-$FeCl_2$; e, FG-$FeSO_4 \cdot 7H_2O$ nanocomposites
628 **Fig. 5** (A) SEM images and (B) particle size distributions of the synthetic nanocomposites: a, FG-$FeCl_3$; b,
629 FG-$Fe_2(SO_4)_3$; c, FG-$FeCl_2$; d, FG-$FeSO_4 \cdot 7H_2O$.
630 **Fig. 6** Cumulative release of iron from the synthetic nanocomposites and original iron salts at predesignated
631 time intervals in SGF (bars represent the standard deviation and data are shown as mean ± SD, $n = 3$).

632 **Table 1** Relevant parameters of four iron loading nanocomposites derived from magnifying experiments

Sample	Appearance	Yield (%)	Iron content (%)					Total carbon (%)	Protein (%)	Total sugar (%)
			Combined	Free	Ferric	Ferrous	Total			
FG	White foam solid	11.92	–	–	–	–	–	39.29 ± 0.03	19.72 ± 0.03	75.09 ± 3.29
FG-$FeCl_3$	Reddish brown powder	48.56	24.96 ± 0.86	0.55 ± 0.13	24.3 ± 0.78	1.21 ± 0.22	25.51 ± 0.99	25.65 ± 0.01	13.72 ± 0.04	60.57 ± 0.73
FG-$Fe_2(SO_4)_3$	Khaki powder	42.32	8.55 ± 0.68	1.81 ± 0.13	9.67 ± 0.61	0.69 ± 0.07	10.36 ± 0.55	31.01 ± 0.04	17.96 ± 0.02	68.43 ± 1.80
FG-$FeCl_2$	Palegoldenrod powder	38.39	3.92 ± 0.12	1.91 ± 0.60	4.31 ± 0.66	1.52 ± 0.18	5.83 ± 0.48	40.06 ± 0.05	18.04 ± 0.05	72.52 ± 3.73
FG-$FeSO_4 \cdot 7H_2O$	Darkkhaki powder	56.08	8.27 ± 0.66	14.55 ± 0.62	1.44 ± 1.41	21.39 ± 0.13	22.83 ± 1.28	16.47 ± 0.10	12.73 ± 0.09	60.05 ± 0.80

633 Data are shown as mean ± SD (n=3), "–" refers to not determined.

634

635 **Table 2** Iron release kinetic models and their parameters (R^2, k, n) in SGF

Parameter	Model	FG-iron nanocomposite				Original iron salt			
		FG-$FeCl_3$	FG-$Fe_2(SO_4)_3$	FG-$FeCl_2$	FG-$FeSO_4 \cdot 7H_2O$	$FeCl_3$	$Fe_2(SO_4)_3$	$FeCl_2$	$FeSO_4 \cdot 7H_2O$
R^2	Zero-order	0.9326	0.8890	0.9219	0.8863	0.7165	0.9273	0.9080	0.9218
	First-order	0.9186	0.7743	0.8820	0.7786	0.5760	0.8218	0.7695	0.7909
	Higuchi	0.8870	0.9607	0.9637	0.9578	0.8315	0.9801	0.9735	0.9809
	Hixson-Crowell	0.9433	0.8187	0.8977	0.8202	0.6241	0.8637	0.8231	0.8202
	Korsmeyer-Peppas	0.9534	0.9659	0.9726	0.9671	0.8384	0.9827	0.9635	0.9729
k	Zero-order (k_0)	0.1473	0.0881	0.0980	0.1134	0.1245	0.1552	0.1520	0.1516
	First-order (k_1)	0.7989	0.2579	0.2020	0.2727	0.2303	0.2821	0.2745	0.2727
	Higuchi (k_H)	0.4342	0.2769	0.3028	0.3562	0.4054	0.4822	0.4756	0.4726
	Hixson-Crowell (k_{HC})	0.1411	0.0593	0.0526	0.0669	0.0614	0.0759	0.0739	0.0726
	Korsmeyer-Peppas (k_{KP})	0.0426	0.2402	0.3617	0.2846	0.4272	0.3663	0.3783	0.3788
n	Korsmeyer-Peppas (k_{KP})	1.6808	0.5946	0.4377	0.6288	0.5738	0.6370	0.6345	0.6243

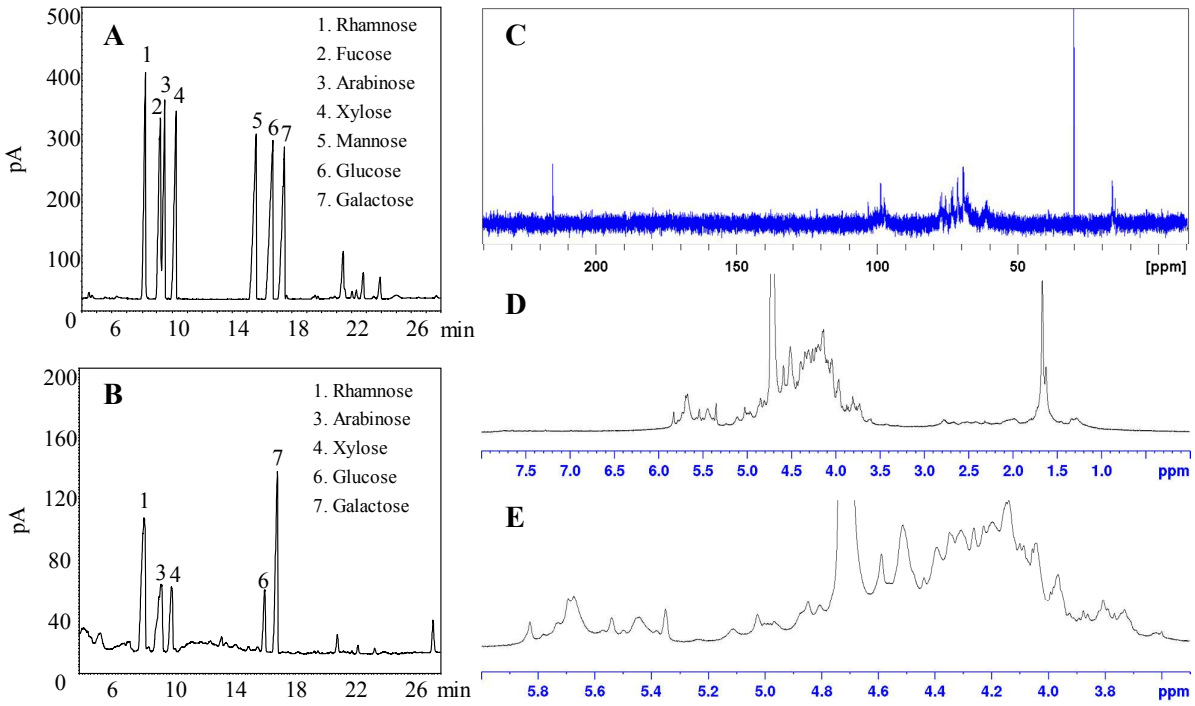
A
1. Rhamnose
2. Fucose
3. Arabinose
4. Xylose
5. Mannose
6. Glucose
7. Galactose
pA
min
B
1. Rhamnose
3. Arabinose
4. Xylose
6. Glucose
7. Galactose
C
[ppm]
D
ppm
E
ppm

Fig. 1

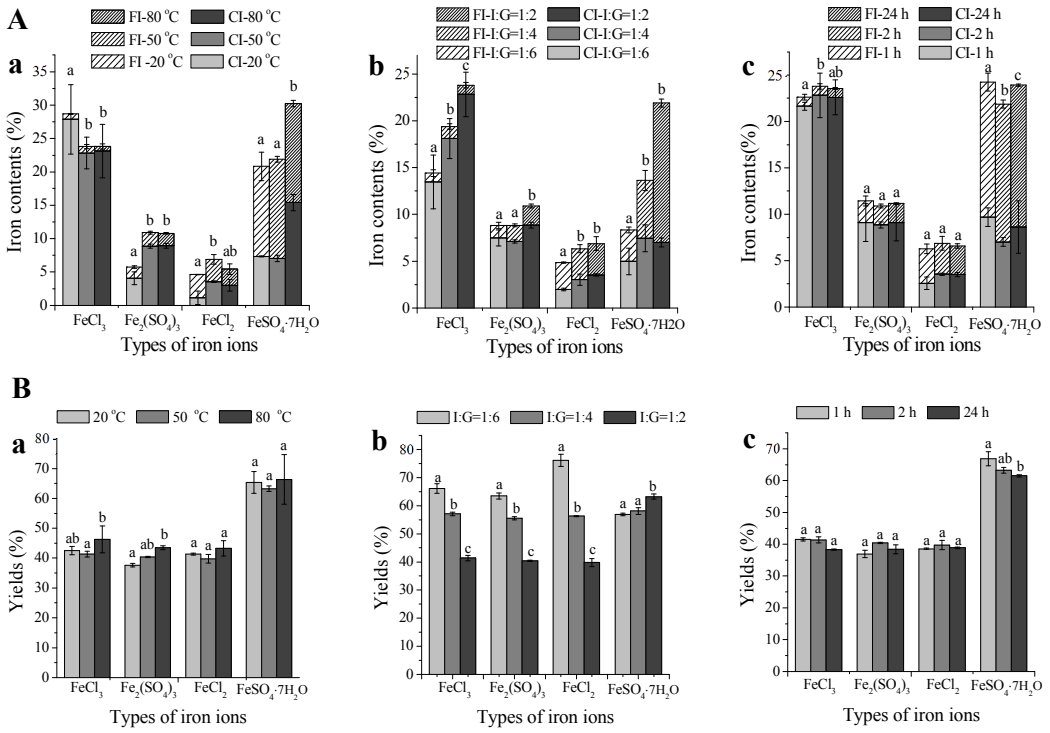
A
FI-80 °C
CI-80 °C
FI-50 °C
CI-50 °C
FI -20 °C
CI-20 °C
FI-I:G=1:2
CI-I:G=1:2
FI-I:G=1:4
CI-I:G=1:4
FI-I:G=1:6
CI-I:G=1:6
FI-24 h
CI-24 h
FI-2 h
CI-2 h
FI-1 h
CI-1 h
Iron contents (%)
Iron contents(%)
Types of iron ions
B
20 °C
50 °C
80 °C
I:G=1:6
I:G=1:4
I:G=1:2
1 h
2 h
24 h
Yields (%)
Types of iron ions

Fig. 2

641

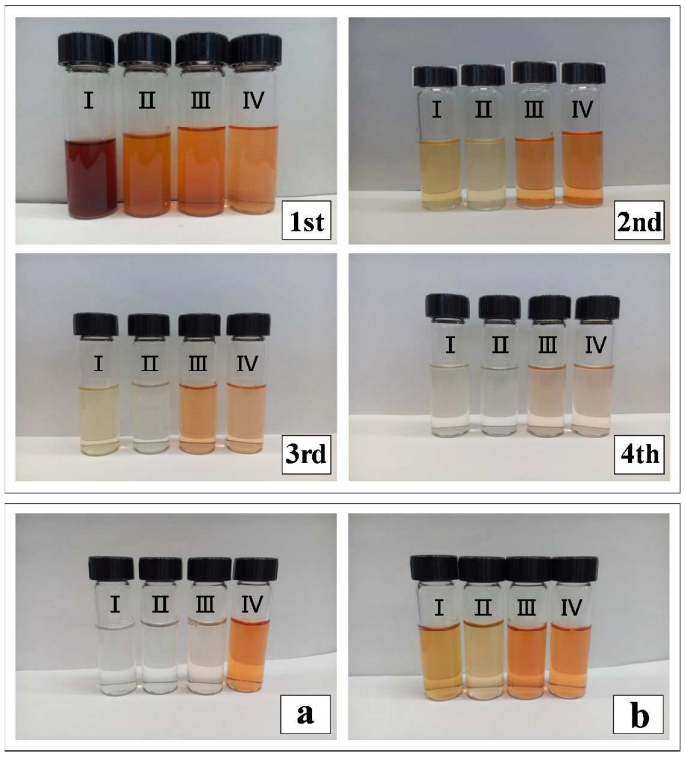

642

643 **Fig. 3**

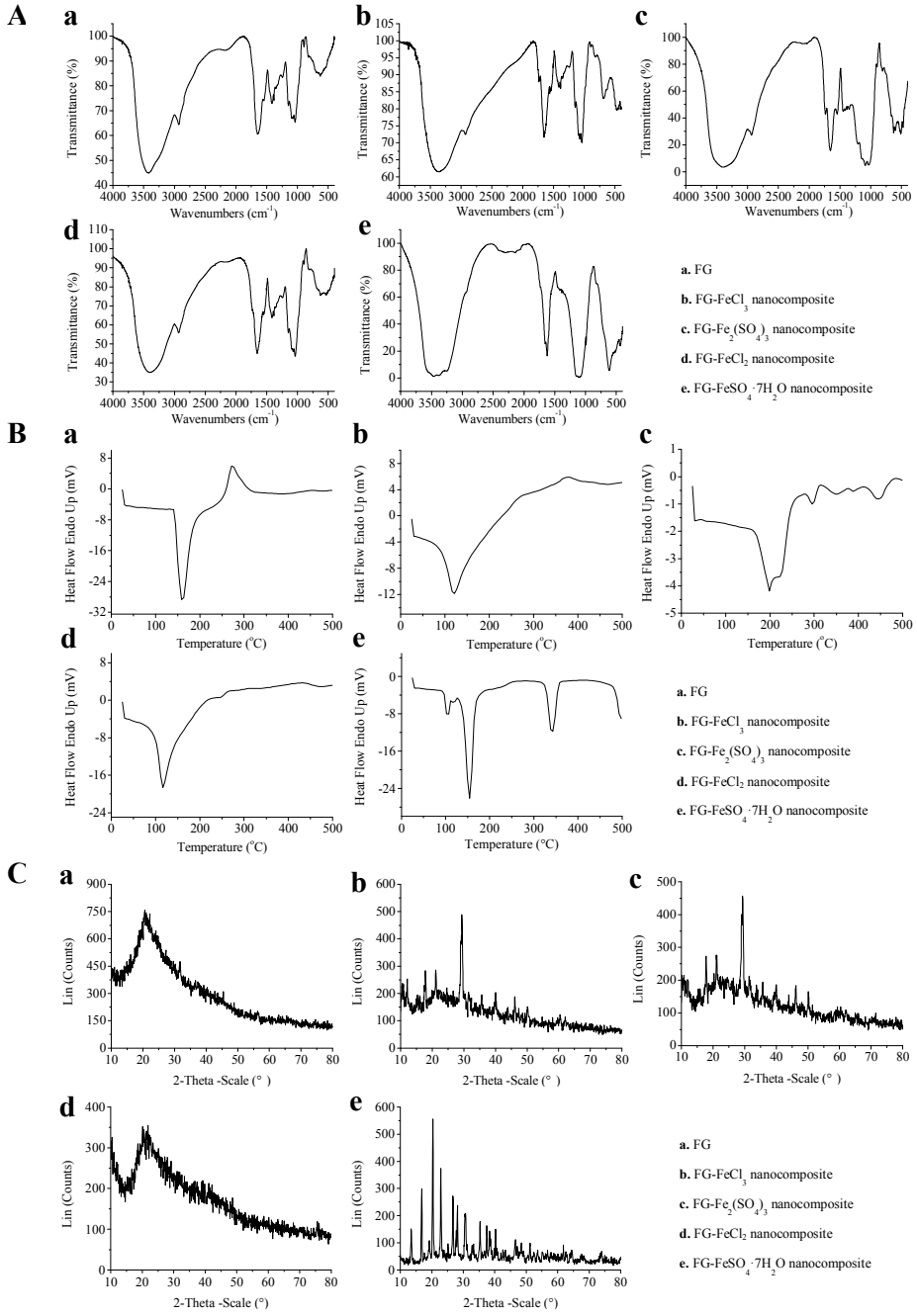
A
a
b
c
d
e
Transmittance (%)
Wavenumbers (cm-1)
a. FG
b. FG-FeCl3 nanocomposite
c. FG-Fe2(SO4)3 nanocomposite
d. FG-FeCl2 nanocomposite
e. FG-FeSO4·7H2O nanocomposite
B
Heat Flow Endo Up (mV)
Temperature (°C)
C
Lin (Counts)
2-Theta -Scale (°)

644

645 **Fig. 4**

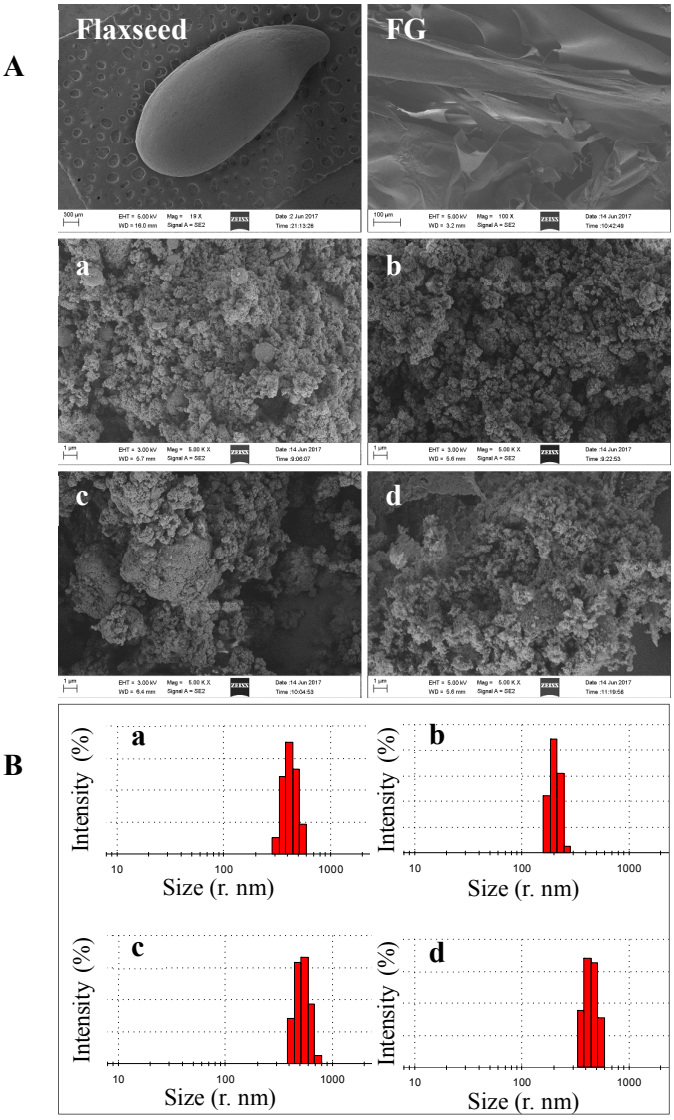

646

647 **Fig. 5**

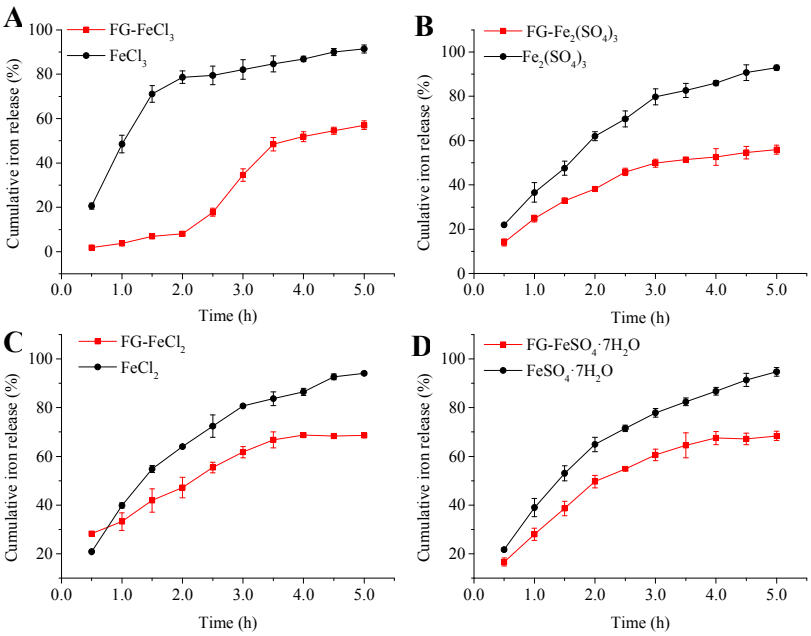
A
FG-FeCl3
FeCl3
Cumulative iron release (%)
Time (h)
B
FG-Fe2(SO4)3
Fe2(SO4)3
Cuulative iron release (%)
Time (h)
C
FG-FeCl2
FeCl2
Cumulative iron release (%)
Time (h)
D
FG-FeSO4·7H2O
FeSO4·7H2O
Cumulative iron release (%)
Time (h)

Fig. 6

651 **Graphical Abstract**

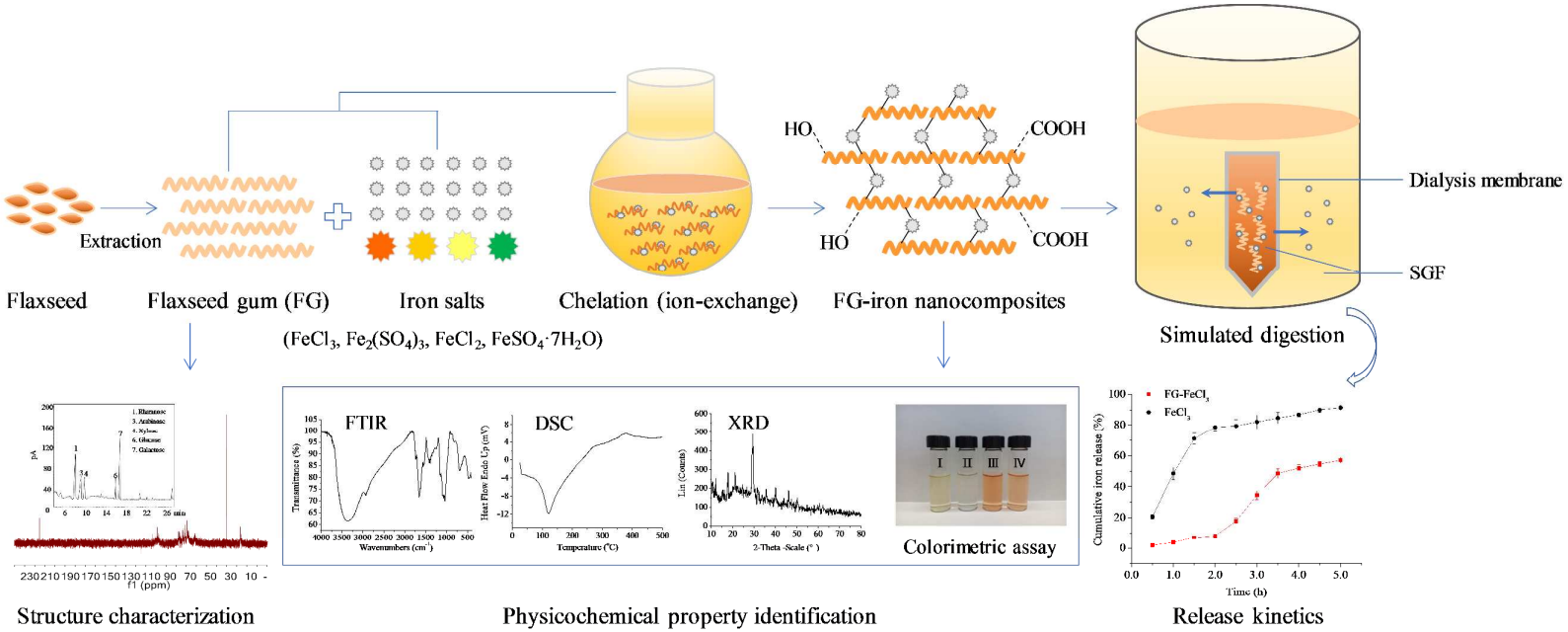

652